Draft version March 29, 2023
Typeset using LaTeX **twocolumn** style in AASTeX63

PLANETESIMAL ACCRETION AT SHORT ORBITAL PERIODS

Spencer C. Wallace[1] and Thomas R. Quinn[1]

[1]*Astronomy Department, University of Washington, Seattle, WA 98195*

ABSTRACT

Formation models in which terrestrial bodies grow via the pairwise accretion of planetesimals have been reasonably successful at reproducing the general properties of the solar system, including small body populations. However, planetesimal accretion has not yet been fully explored in the context of the wide variety of recently discovered extrasolar planetary systems, particularly those that host short-period terrestrial planets. In this work, we use direct N-body simulations to explore and understand the growth of planetary embryos from planetesimals in disks extending down to $\simeq 1$ day orbital periods. We show that planetesimal accretion becomes nearly 100 percent efficient at short orbital periods, leading to embryo masses that are much larger than the classical isolation mass. For rocky bodies, the physical size of the object begins to occupy a significant fraction of its Hill sphere towards the inner edge of the disk. In this regime, most close encounters result in collisions, rather than scattering, and the system does not develop a bimodal population of dynamically hot planetesimals and dynamically cold oligarchs, like is seen in previous studies. The highly efficient accretion seen at short orbital periods implies that systems of tightly-packed inner planets should be almost completely devoid of any residual small bodies. We demonstrate the robustness of our results to assumptions about the initial disk model, and also investigate the effects that our simplified collision model has on the emergence of this non-oligarchic growth mode in a planet forming disk.

1. INTRODUCTION

Planetesimal accretion is a key phase in the terrestrial planet growth process, bridging the gap from kilometer-sized bodies up to roughly moon-sized objects known as planetary embryos. In the earliest stages of the planet formation process, beginning from μm sizes, aerodynamic forces dominate the growth and evolution of the solids and statistical models (Johansen et al. 2014; Birnstiel et al. 2016) are appropriate to describe how these numerous, small bodies coagulate.

Due to the internal pressure support of the gas disk, the gas itself orbits at sub-Keplerian speed and exerts a headwind on any solids large enough to decouple from the gas (Weidenschilling 1977). Around a meter in size, this headwind is maximally effective at sapping away orbital angular momentum, and planet-building material can fall onto the central star on catastrophically short timescales (Weidenschilling 1977; Nakagawa et al. 1986). Additionally, laboratory experiments suggest that collisions between mm- to cm- sized solids tend to result in bounces or destruction, rather than continued growth (Blum & Münch 1993; Colwell 2003; Beitz et al. 2011).

For these reasons, a number of mechanisms to radially concentrate solids in a planet-forming disk have been proposed to facilitate fast growth from mm to km sizes (Johansen et al. 2007; Lyra et al. 2008; Bai & Stone 2010) in order to surmount these barriers. Interestingly, formation models for the short-period multiplanet systems revealed by Kepler (Fabrycky et al. 2014) also seem to require enhanced concentrations of planet-building material to reproduce the observed architectures (Raymond et al. 2007; Hansen & Murray 2012).

Regardless of how the mm- to km-sized growth barriers are surmounted, gravity begins to dominate and aerodynamic gas drag plays an increasingly unimportant role beyond this size. During this phase, collision cross sections are enhanced as gravitational focusing (Safronov 1969) acts to bend the trajectories of bodies undergoing close encounters. Because gravitational focusing becomes more effective as bodies grow larger, a period of runaway growth occurs (Wetherill & Stewart 1989; Kokubo & Ida 1996; Barnes et al. 2009) and a power law spectrum of masses develop. Eventually, the largest bodies (known as oligarchs) dynamically heat the remaining planetesimals, severely limiting further growth (Kokubo & Ida 1998). The final outcome of this phase is a bimodal population of dynamically cold oligarchs, surrounded by dynamically hot, difficult to accrete residual planetesimals. Lines of evidence suggest that the asteroid belt **(Bottke et al. 2005; Morbidelli et al. 2009)**, Kuiper belt **(Levison et al. 2008; Shepard & Trujillo 2010)** and the Oort cloud **(Levison**

et al. 2011) are largely composed of the leftovers of this stage of planet formation.

After a long period of quiescence, the collection of embryos and remaining planetesimals undergo a large-scale instability (Chambers & Wetherill 1998). As a consequence of the instability, the oligarchics are no longer on isolated, stable orbits and coalesce to form Earth-sized planets through a series of extremely energetic giant impacts (Kokubo & Ida 2002; Raymond et al. 2005, 2006).

Due to the relative ease of modeling the early dust coagulation phases and the final giant impact phase, these steps in the terrestrial planet formation process have received most of the attention in the literature. The planetesimal accretion phase, which we will focus on in this paper, is more difficult and expensive to model because there are too many particles to directly track with traditional N-body codes, while the gravitational interactions between the **few massive bodies produced by the runaway growth phase (Ida & Makino 1993; Kokubo & Ida 1995, 1998) render statistical methods inappropriate**. Due to computational expense, N-body simulations of planetesimal accretion are usually modeled in a narrow ring (Kokubo & Ida 1996, 1998), and the results and timescales are then scaled to suit whatever relevant orbital period is being studied. N-body simulations of terrestrial planet assembly typically begin with a series of neatly spaced oligarchs, whose mass varies smoothly with orbital period. As we will show in this paper, oligarchic growth does not scale to arbitrarily short orbital periods.

Given that Systems of Tightly-packed Inner Planets (STIPs) appear to be a common outcome of planet formation (Latham et al. 2011; Lissauer et al. 2011; Rowe et al. 2014), understanding exactly how solids accumulate at short orbital periods is crucial. Although gas-disk driven migration of the planets themselves is often invoked to explain the observed architectures **(Izidoro et al. 2017, 2021)**, we will focus on an in-situ model in this paper. That is, once the planetesimals themselves form, they largely stay in place, and any subsequent large-scale movement of the solids are the result of mutual gravitational interactions. The focus of this work will be to understand how the outcome of the planetesimal accretion process scales with orbital period by using a high-powered N-body code to directly follow the growth and evolution of the planetesimals across a wide range of orbital periods (1 to 100 days). In doing so, we will assess whether the typical initial conditions (fully formed, evenly spaced protoplanets, e.g. Raymond et al. (2006)) used in studies of terrestrial planet formation are actually appropriate for understanding STIPs.

In section 2 we provide an overview of the theory behind planetesimal accretion and show that assumptions used to derive the well-known modes of growth are only valid at sufficiently long orbital periods. We then motivate the need for N-body simulations to study this problem and describe the code used, along with how our initial conditions were constructed in section 3. In section 4, we present a parameter study of planetesimal accretion using a series of simulations of narrow annuli that exhibit both oligarchic and non-oligarchic growth. In section 5 we present a set of simulations starting with a wide planetesimal disk and demonstrate that a transition between accretion modes occurs at moderately small orbital periods. Next, we assess the impact of simplifications made to our collision model on this result in section 6. In section 7, we discuss the implications of this multimodal accretion behavior throughout the disk for planet formation models and conclude.

2. OVERVIEW OF PLANETESIMAL ACCRETION

2.1. *Oligarchic and Runaway Growth*

We begin our analysis by considering a disk of equal mass planetesimals with radius r_{pl}, mass m_{pl} and surface density Σ_{pl}. The collision rate in the vicinity of an orbit defined by Keplerian frequency Ω can be written as $n\Gamma v$, where $n = \Sigma_{pl}\Omega/2m_{pl}v$ (where we have assumed that the scale height of the planetesimal disk goes as $2v/\Omega$). Γ describes the effective collision cross section and v is the typical encounter velocity between planetesimals. For a swarm of planetesimals on randomly oriented orbits, v is typically taken to the rms velocity, which can be related to the eccentricity and inclination distribution (e, i) in the following way (Lissauer & Stewart 1993):

$$\left\langle v^2 \right\rangle^{1/2} = \left(\frac{5}{4} \left\langle e^2 \right\rangle^{1/2} + \left\langle i^2 \right\rangle^{1/2} \right) v_k. \tag{1}$$

Assuming that every collision results in a perfect merger, the growth rate of a planetesimal is given by

$$\frac{1}{M}\frac{dM}{dt} = \frac{\Sigma\Omega}{2m_{pl}}\Gamma. \tag{2}$$

In the case where the collision cross section depends only on the physical size of the planetesimals, the growth scales sub-linearly with mass and the mass distribution is expected to evolve in an "orderly" fashion, in which mass ratios between bodies tend toward unity. However, bodies larger than ~ 100 km in size are expected to exert a significant gravitational force on each other during encounters and the collision cross section depends on both the size of the bodies and their encounter velocities. In this case, $\Gamma = \pi r_{pl}^2 \left(1 + v_{esc}^2/v^2\right)$ (Safronov 1969), where

v_{esc} is the escape velocity from the two bodies at the point of contact.

In the limit that $v_{esc} \gg v$, it can be shown that $dM/dt \propto M^{4/3}$, which implies a runaway scenario where growth accelerates with mass. This mode of growth was confirmed with N-body simulations by Kokubo & Ida (1996) and appears necessary to construct protoplanets within the lifetime of a protoplanetary disk **(Lissauer 1987), although one should note that pebble accretion (Lambrechts & Johansen 2012, 2014; Bitsch et al. 2015) is a viable alternative scenario**. Due to the velocity dependence of the gravitational focusing effect, it is not clear how ubiquitous this mode of growth is. In particular, encounter velocities at short orbital periods will be rather large (because $v \sim v_k$) and the $v_{esc} \gg v$ condition may not always be satisfied. The effect that a dynamically hot disk has on runway growth will be examined in detail in section 4.

An important feature is missing from the model described above, which limits its applicability at late times. Gravitational stirring, which converts Keplerian shear into random motion, raises the typical encounter velocity between planetesimals over time (Weidenschilling 1989; Ida 1990) and diminishes the effectiveness of gravitational focusing. As the mass spectrum of the system evolves away from uniformity, these velocity differences become even more pronounced. As the system evolves, it tends toward a state of energy equipartition where $v \sim m^{1/2}$. For a system of equal mass bodies in which encounters are driven by random motions rather than Keplerian shear (dispersion dominated), the timescale for gravitational stirring is described by the two-body relaxation time (Ida & Makino 1993)

$$t_{relax} = \frac{v^3}{4\pi n G^2 m_{pl}^2 \ln \Lambda}, \tag{3}$$

where $\ln \Lambda$ is the Coulomb logarithm, typically taken to be ≈ 3 **for a planetesimal disk (Ida 1990; Stewart & Ida 2000)**. Despite the fact that the behavior of gravitational stirring is well-described by a two-body formula, (Ida & Makino 1993) found that the stirring in a planetesimal disk is actually driven by close encounters, which requires a three-body formalism. As we will show in section 4, gravitational stirring effectively shuts off when the Hill sphere of a body becomes comparable to its physical size. In this case, close encounters tend to result in collisions, and the main pathway for energy exchange between planetesimals and growing protoplanets is unable to operate.

Kokubo & Ida (1998) showed that **the runaway growth process described above** is actually self-limiting. As the runaway bodies develop, they become increasingly effective at **dynamically** heating the remaining planetesimals, which diminishes the gravitational focusing cross sections and throttles the growth rate. Around the time that the mass of the runaway bodies exceeds the mass of the planetesimals by a factor of $\sim 50-100$ (Ida & Makino 1993) a phase of less vigorous "oligarchic" growth commences, in which the largest bodies continue to accrete planetesimals at similar rates, independent of mass.

The picture described above relies upon **a** crucial assumption, which is that the mass distribution evolves slowly enough for gravitational stirring to maintain energy equipartition. In other words, the relaxation timescale must remain short relative to the **collision** timescale. For typical conditions near the terrestrial region of the solar system, this timescale condition is satisfied. Due to the steep dependence of the relaxation time on encounter velocity, however, this condition can easily be violated at shorter orbital periods.

In figure 1, we show the ratio between the relaxation and collision timescale for a population of equal-mass planetesimals as a function of orbital period. Here, the encounter velocity is described by equation 1. For simplicity, we assume that $\langle e^2 \rangle^{1/2} = 2 \langle i^2 \rangle^{1/2}$ (Ida et al. 1993) and that the eccentricity dispersion is constant with orbital period. The eccentricity dispersion is scaled by the Hill factor $\left(m_{pl}/3M_\star\right)^{1/3}$ such that $e_h = 1$ corresponds to the boundary between shear and dispersion dominated encounters. The horizontal dashed line indicates where $t_{relax} = t_{coll}$. The timescale criterion for oligarchic growth is only satisfied in regions where the disk is sufficiently dynamically cold and the orbital period is sufficiently long. In sections 4 and 5 we will explore the behavior and outcome of planetesimal accretion in regions where this criterion is *not* satisfied.

2.2. *Planetesimal Size and Extent of Hill Sphere*

In the formalism described above, the mass and velocity distribution of the bodies are both a function of time. Due to the interdependence of these quantities, it is not clear whether the **ratio between the relaxation and collision timescales will remain constant** as the oligarchs develop. In the case of the solar system, $t_{relax} \ll t_{coll}$ likely continued to remain true, otherwise runaway growth would have consumed all of the small bodies and there would be nothing left to populate the asteroid or Kuiper belt. In the case where $t_{coll} \ll t_{relax}$, however, it is not clear how the system might evolve.

An insight into the expected behavior in this regime can be gained by defining a dimensionless parameter, α, which is the ratio between the physical size of a body

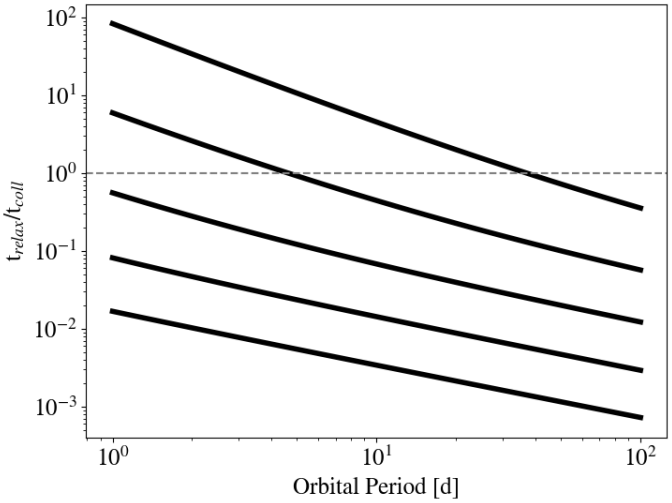

Figure 1. The ratio between the two-body relaxation and collision timescale for a population of equal-mass planetesimals with an internal density of 3 g cm^{-3} and an eccentricity dispersion characterized by e_h. Only in regions where $t_{relax} \ll t_{coll}$ can the velocity distribution respond to changes in the mass of the bodies such that oligarchic growth can operate. This condition is no longer satisfied for a dynamically hot disk at sufficiently short orbital periods.

and its Hill radius, r_h

$$\alpha = \frac{r_{pl}}{r_h} = \frac{1}{a}\left(\frac{9M_\star}{4\pi\rho_{pl}}\right)^{1/3}, \quad (4)$$

where a is the semimajor axis of the body and ρ_{pl} is its bulk density. Assuming that the bulk density stays constant as bodies collide and grow, and that no large-scale migration occurs, the scaling of both r_{pl} and r_h as $m_{pl}^{1/3}$ means that α will be constant with time. For a composition of ice and rock, α is small for any presently populated region of the solar system ($\alpha \sim 10^{-2}$ near Earth and $\alpha \sim 10^{-4}$ in the Kuiper belt). As one moves closer to the sun, α becomes larger than 1, which implies that the Hill sphere of a body becomes smaller than its physical size.

The magnitude of α controls the relative importance of gravitational scattering and collisions in driving the evolution of the planetesimal disk. When α is small, most close encounters will result in a gravitational interaction, moving the system toward a state of relaxation. If, however, the Hill sphere is largely filled by the body itself, these same encounters will instead drive evolution of the mass spectrum. Because α stays constant with mass, the boundary in the disk where collisions or gravitational encounters dominate, will stay static with time.

We also introduce a second dimensionless quantity, which relates the physical size of the bodies to the velocity state of the system

$$\beta = \frac{r_{pl}}{r_g}. \quad (5)$$

where $r_g = Gm_{pl}/v^2$ is the gravitational radius of a body (see eq 4.1 of Ida (1990)). Encounters between bodies inside of a distance of r_g result in significant deflections of their trajectories. It should be noted that the gravitational focusing enhancement factor v^2/v_{esc}^2 is equal to 1 for $\beta = 1$. In the case where r_g is smaller than the size of a planetesimal, the gravitational focusing enhancement factor will be between 0 and 1 and the collision cross section is mostly set by the geometric value. **For very large values of r_g ($\beta \gg 1$), the effective collision cross section is almost entirely set by gravitational scattering.**

These scaling considerations motivate the range of parameters we choose for the numerical experiments presented in the next section, where we aim to understand where and when runaway and oligarchic growth can operate.

3. NUMERICAL METHODS

We use the tree-based N-body code ChaNGa[1] to model the gravitational and collisional evolution of a swarm of planetesimals. ChaNGa is written using the CHARM++ parallel programming language and has been shown to perform well on up to half a million processors (Menon et al. 2015) and can follow the evolution of gravitationally interacting collections of up to billions of particles. Using a modified Barnes-Hut tree with hexadecapole expansions of the moments to approximate forces, ChaNGa integrates the equations of motion using a kick-drift-kick leapfrog scheme. For all of the simulations presented in this paper, we use a node opening criteria of $\vartheta_{BH} = 0.7$. Additional information about the code is available in (Jetley et al. 2008; Menon et al. 2015).

Using the neighbor-finding algorithm in ChaNGa, originally designed for SPH calculations, we have recently implemented a solid body collision module in the code. This work is largely based on the solid-body collision implementation in PKDGRAV, which is described in Richardson (1994) and Richardson et al. (2000). To summarize, imminent collisions are detected during the "drift" phase by extrapolating positions of bodies forward in time, using the velocity calculated at the open-

[1] A public version of ChaNGa can be downloaded from http://www-hpcc.astro.washington.edu/tools/ChaNGa.html

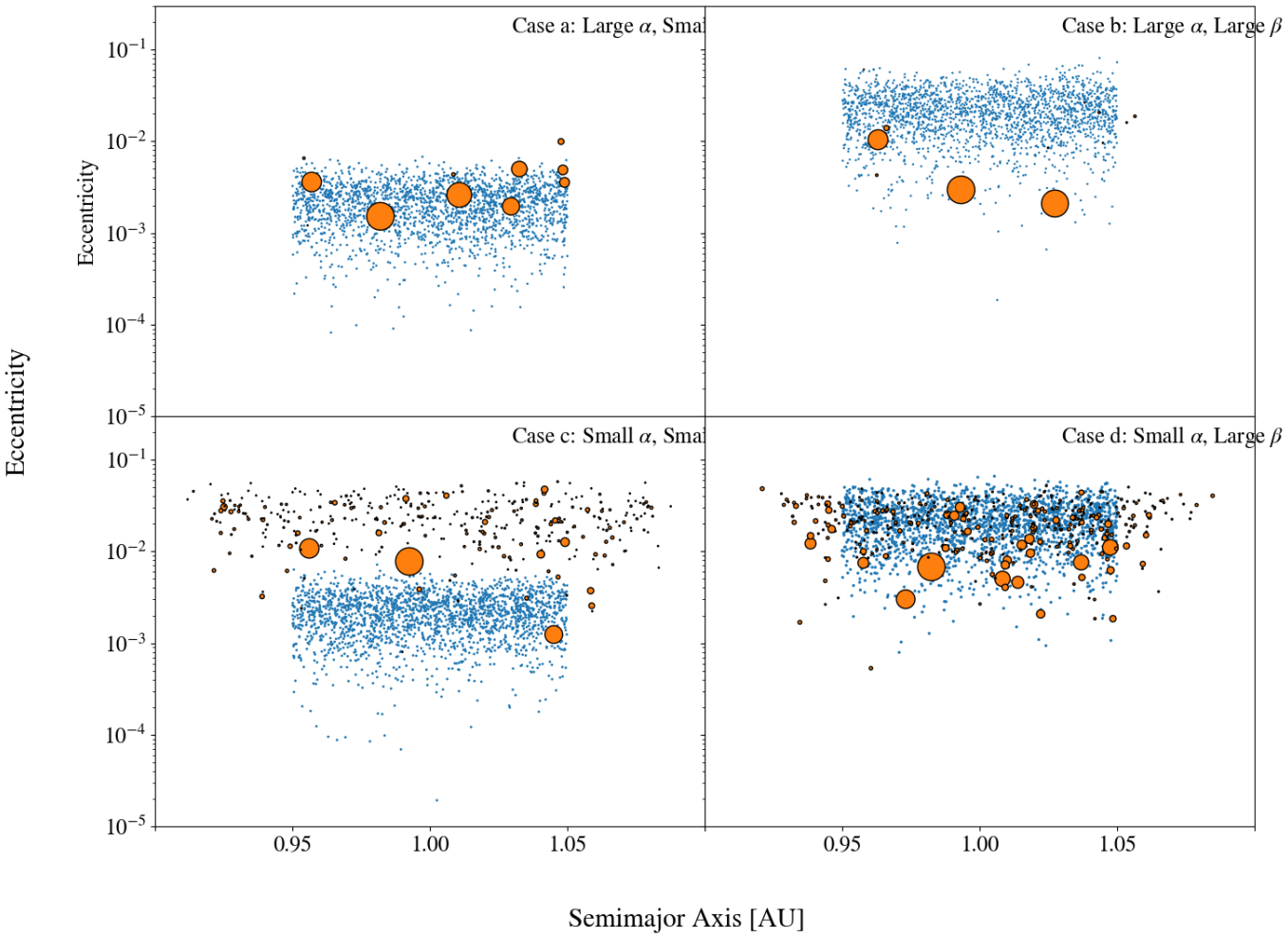

Figure 2. The initial (blue) and final (orange) states of the narrow annulus simulations described in section 4. Relative masses of the bodies are indicated by point size. In the case of large α, almost no residual planetesimal population remains. Regardless of the initial choice of β, the protoplanets that form attain similar eccentricities.

ing "kick". For each body, any neighboring particles which fall within a search ball of radius $2\Delta T v + 2r_{pl}$, where ΔT is the current timestep size for the particle and v is magnitude of its heliocentric velocity, are tested for an imminent collision. In the case that a collision is detected, the particles are merged into a single larger body, which is given the center of mass position and velocity of the two **parents**. Resolving a collision can produce another imminent collision, so collisions are handled one-by-one and another full collision check is run after the previous event is resolved. For a more detailed description of the collision module in ChaNGa, see (Wallace & Quinn 2019). Particles are advanced on individual timesteps chosen as a power of two of a base timestep. The timestep for an individual particle is based on an estimate of the gravitational dynamical time determined by the minimum of $\sqrt{d_{node}^3/(G(M_{node}+m_{pl}))}$ across all nodes in the tree that are accepted by the Barnes-Hut opening criterion. Here d_{node} is the distance from the planetesimal to the center of mass of the tree node and M_{node} is the total mass of the tree node. For nearby particles M_{node} is replaced with the mass of the nearby particle.

4. NARROW ANNULUS SIMULATIONS

We begin by **exploring the outcome of planetesimal accretion in different parts of the** (α, β) **parameter space.** The choices of α and β are motivated by two questions raised in section 2. 1) Does runaway growth still operate when the condition that $v \ll v_{esc}$ is not satisfied? 2) How does planetesimal accretion proceed when the planetesimals themselves occupy a significant fraction of their Hill spheres?

To answer these questions, we run a series of simulations in which a narrow annulus of planetesimals orbits a star. The values of α and β are varied individually.

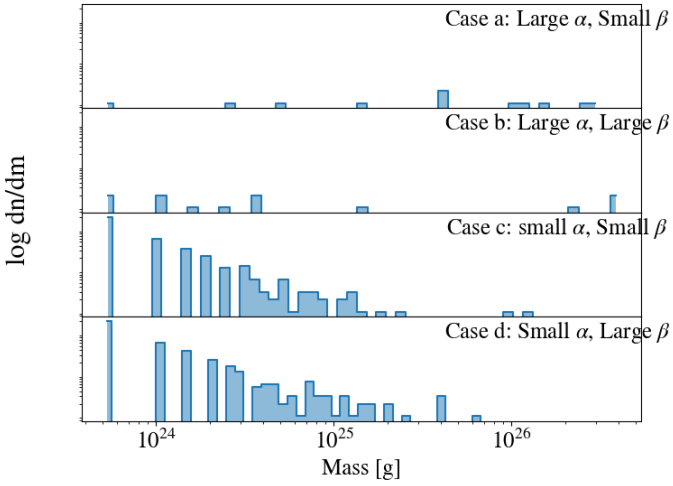

Figure 3. The final state of the mass distributions for the narrow annulus simulations described in section 4. For small α, a few embryos form alongside a power law tail of planetesimals. For larger values of α, the mass distribution stops being bimodal. As in the previous figure, the initial choice of β does not appear to have any meaningful impact on the end result.

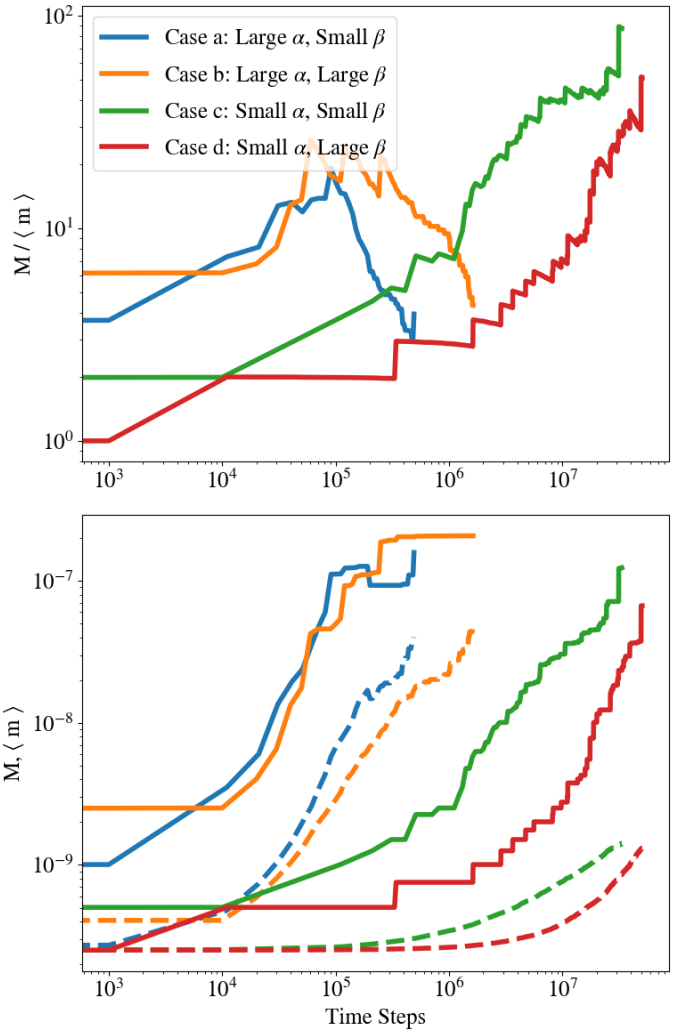

Figure 4. Top: The evolution of the ratio between the maximum and mean mass for the four simulations presented in section 4. The runaway growth phase can be identified by a positive trend in this ratio. For all values of α, an increase in β has the effect of delaying runaway growth. **Bottom: The evolution of the maximum (solid lines) and mean (dashed lines) shown individually.**

4000 planetesimals with individual masses of 5×10^{23} g are placed with semimajor axes drawn **from a uniform distribution** between 0.95 and 1.05 AU about a 1 $M_\odot$ star. The argument of perihelion, ω, longitude of ascending node, Ω, and mean anomaly, M, for each body is drawn from a uniform distribution $\in [0, 2\pi)$. The inclinations and eccentricities are drawn from a Rayleigh distribution with $\langle i^2 \rangle = 1/2 \langle e^2 \rangle$ (Ida et al. 1993).

In the "fiducial" case, we give the bodies a bulk density of 3 g cm^{-3}, and $\langle e^2 \rangle^{1/2} = 4e_h$, which corresponds to $\alpha = 3.6 \times 10^{-2}$ and $\beta = 3.4 \times 10^{-3}$. These parameters are chosen to match the initial conditions of Kokubo & Ida (1998), which gave rise to oligarchic growth. To vary the value of α, we alter the bulk density of the particles. In the high-α case, the bulk density is reduced by a factor of ∼ 7100, which produces $\alpha = 1$. **In this case, a planetesimal completely fills its Hill sphere, and one should expect no strong gravitational scattering to occur.** To vary β, the eccentricity dispersion is increased. For the high-β case, $\langle e^2 \rangle^{1/2}$ is increased to $1500e_h$, which corresponds to $\beta = 15,000$. **This choice of β places the system firmly in the $v > v_{esc}$ regime, while still allowing growth to occur in a reasonable number of timesteps.**

In all cases, the simulations are evolved with a base timestep of 1.7 days, which corresponds to 3% of an orbital dynamical time $\sqrt{a^3/GM_*}$. Due to the vastly differing growth timescales in each case, a simulation is stopped when the growth of the most massive body flattens out. In figure 2, we show the a-e distribution of bodies in the initial (blue) and final (orange) snapshots from each of the 4 simulations. The size of the points indicates the relative masses of the bodies. Only **with small α (case c, d)** does a residual population of dynamically hot planetesimals develop. The lack of high eccentricity planetesimals in the large α **(case a, b) simulation** suggests that most encounters result in accretion rather than scattering. **For** large β **(case b, d)**, the **growing** protoplanets and end up in a dynamically cool state, **relative** with the initial conditions. This is due to kinetic energy being lost as particles inelastically

collide. One last point we note is the difference between the eccentricities of protoplanets in the large α, large β **(case b)** and the small α, large β **(case d) simulation**. The dynamically cooler result of the **former** case is likely due to the dominant role that inelastic collisions play here.

In figure 3, we show the mass distribution of bodies from the final snapshot in each of the four **simulations**. In addition to leaving fewer residual planetesimals, the large α **(case a, b)** simulations produce **embryos that are a factor of a few larger**. Despite the vastly different encounter velocities of each population of bodies, the initial size of β (so long as bodies remain in the dispersion-dominated regime) appears to have no significant effect on the final distribution of masses.

To investigate whether any of these planetesimal rings underwent runaway growth, we examine the time evolution of the maximum and mean masses in each simulation. The ratio $M/\langle m \rangle$ is plotted in **the top panel of** figure 4. **Here**, a positive slope indicates that the quantities are diverging (i.e. the growth rate is accelerating with mass). This behavior is evident in all four cases. Even with a large β, where the effective collision cross section is nearly equal to the geometric value, runaway growth still appears to operate. The ubiquity of the early positive trends in this figure suggests that as bodies collide and grow, the relative difference in gravitational focusing factors between bodies is what drives the system towards runaway growth, no matter how close the collision cross sections lie to the geometric value. Although larger encounter velocities lengthen the growth timescales, runaway growth appears to be inevitable, so long as gravity is the dominant force in the system. For large α **(case a, b)**, the curves in this figure eventually turn over and begin to decline. **In the bottom panel of figure 4, we separately show the evolution of the maximum (solid lines) and mean (dashed lines) mass for each case. Here, it is evident** that **the turnover in** $M/\langle m \rangle$ is driven by an increase in the average mass as the planetesimal population becomes depleted. One should expect that the same thing will eventually occur for small α, although many more timesteps are required to begin to run out of planetesimals.

Additionally, these results suggest that the value of α, which is a function of only the initial conditions, controls the qualitative outcome of accretion. Across most of a planet-forming disk, α is small, and frequent gravitational encounters between the growing bodies will facilitate oligarchic growth. In the dispersion-dominated regime, close encounters drive the stirring between planetesimals and embryos (Weidenschilling 1989; Ida 1990).

Table 1. Summary of Full Disk Simulations Run

Name	m_{pl}^{a}	N_{pl}^{b}	A^{c}	δ^{d}
fdHi	5×10^{22}	903,687	100	1.5
fdHiShallow	5×10^{22}	903,687	100	0.5
fdHiSteep	5×10^{22}	903,687	100	2.5
fdLo	5×10^{22}	45,185	1	1.5

NOTE
[a] Planetesimal mass [g]
[b] Number of planetesimals
[c] Solid surface density normalization (relative to MMSN)
[d] Solid surface density power law index

When $\alpha \ll 1$, the Hill sphere of a body is mostly empty space and the majority of close encounters result in viscous stirring, rather than accretion. In the opposite regime, we observe that runaway growth still occurs, but nearly all of the planetesimals are consumed by the forming protoplanets, rather than being scattered onto higher eccentricity orbits, where they would otherwise remain as a remnant of the early stages of planet formation (Kokubo & Ida 1998, 2000).

5. FULL DISK SIMULATION

5.1. *Initial Conditions*

Motivated by the qualitative dependence of accretion on α, we next investigate whether this highly efficient, non-oligarchic growth should be expected to operate near the innermost regions of a typical planet-forming disk. Given that N-body simulations of short-period terrestrial planet formation typically begin with a chain of neatly-spaced, isolation mass (see Kokubo & Ida (2000) eq. 20) protoplanets, it is pertinent to determine whether the high α growth mode we revealed in the previous section invalidates this choice of initial conditions.

Given the dearth of short-period terrestrial planets observed around M stars (e.g. TRAPPIST-1 **(Gillon et al. 2016, 2017; Agol et al. 2021)**), we chose to model the evolution of a series of wide planetesimal disks, which span from 1 to 100 days in orbital period, orbiting a late-type M star of mass 0.08 $M_{\odot}$. For a population of planetesimals with a bulk density of 3 g cm^{-3}, this orbital period range corresponds to $\alpha \in (0.7, 0.05)$. By simultaneously modeling a broad range of orbital periods, we can determine the critical value of α that divides these two modes of accretion, and also explore how the oligarchic/non-oligarchic accretion boundary affects the resulting distribution of protoplanets.

Four wide-disk simulations are run in total (see table 1). In each case, the solid surface density follows a power

law profile

$$\Sigma(r) = 10 \text{ g cm}^{-2} \times A \left(\frac{M_*}{M_\odot}\right) \left(\frac{r}{1 \text{ AU}}\right)^{-\delta} \quad (6)$$

where M_* is the mass of the central star, $\Sigma_{MMSN} = 10$ g cm^{-2} is the surface density of the minimum-mass solar nebula (Hayashi 1981) at 1 AU, A is an enhancement factor and δ is the power law index. In the first case (fdHi), we model a disk that follows a MMSN power law slope ($\delta = 1.5$), with the overall normalization enhanced by a factor of 100. This choice of normalization for the solid surface density profile appears necessary in order to reproduce many observed short period terrestrial worlds in-situ (Hansen & Murray 2012). Additionally, we vary the power law index (fdHiShallow, fdHiSteep) and overall normalization (fdLo) of $\Sigma(r)$.

In all cases, the eccentricities and inclinations of the bodies are randomly drawn from a Rayleigh distribution, with $\langle e^2 \rangle^{1/2} = 2 \langle i^2 \rangle^{1/2} = e_{eq}$ (Ida & Makino 1993). The value of e_{eq} is chosen such that the timescales for viscous stirring and aerodynamic gas drag on the planetesimals are in equilibrium. The viscous stirring timescale is given by Ida & Makino (1993) as

$$\tau_{vs} = \frac{\langle e^2 \rangle}{d \langle e^2 \rangle / dt} \approx \frac{1}{40} \left(\frac{\Omega^2 a^3}{2 G m_{pl}}\right)^2 \frac{4 m_{pl} \langle e^2 \rangle^2}{\Sigma a^2 \Omega}, \quad (7)$$

where Ω, a and e are the orbital frequencies, semimajor axes and eccentricities of the individual planetesimals. In the Stokes regime, the gas drag timescale is given by Adachi et al. (1976) as

$$t_s = \frac{2 m_{pl}}{C_D \pi r_{pl}^2 \rho_g v_g}, \quad (8)$$

where C_D is a drag coefficient of order unity, ρ_g is the local gas volume density and v_g is the headwind velocity of the gas experienced by the planetesimal. The local gas volume density is given by

$$\rho_g = \frac{\Sigma_g}{\sqrt{2\pi} h_g} \exp\left[-z^2 / \left(2 h_g^2\right)\right], \quad (9)$$

where Σ_g is the gas surface density (taken to be 240 times the solid surface density (Hayashi 1981), $h_g = c_s/\Omega$ is the local gas scale height and z is the height above the disk midplane. The sound speed profile is given by $c_s = \sqrt{k_B T(r) / (\mu m_H)}$, where k_B is Boltzmann's constant, $T(r) = T_0 r^{-Q}$, $\mu = 2.34$ and m_h is the mass of a hydrogen atom. For a protoplanetary disk around a typical M star, $T_0 = 148$ K and $Q = 0.58$ (Andrews & Williams 2005).

Finally, the headwind velocity of the gas, due to the fact that the gas disk is pressure supported, is given by

$$v_g = v_k \left[1 - \sqrt{Q c_s^2 / v_k^2}\right], \quad (10)$$

where v_k is the local Keplerian velocity. As in section 4, the argument of perihelion ω, longitude of ascending node Ω, and mean anomaly M for the planetesimals are drawn from a uniform distribution $\in [0, 2\pi)$.

5.2. *Gas Drag Force*

In addition to the mutual gravitational forces, a Stokes drag force due to the the gas disk is applied to each particle, following the prescription described in section 2.2.1 of Morishima et al. (2010). For the initial mass planetesimals, the stopping time (see equation 8) at the inner edge of the disk is roughly 100 yr. Although this is a few orders of magnitude shorter than the integration time of the simulations, the Stokes drag force plays a fairly insignificant role as the bodies grow via mutual collisions. By the time the bodies reach isolation mass (roughly a tenth of an Earth mass), the stopping time at the inner disk edge exceeds 50,000 years. Although the aerodynamic gas drag is not expected to significantly alter the final protoplanet distribution, we include its effects here to be self-consistent with the initial conditions, which were constructed by balancing the effects of viscous stirring with gas drag.

5.3. *Timestepping Criterion*

In the case of the fdHi simulation, there are nearly 1 million particles, whose orbital periods vary by two orders of magnitude. Because the interaction timescales near the inner edge of the disk are exceedingly short, a fixed timestep size would required a prohibitively large number of steps to follow planetesimal growth throughout the entire disk. For this reason, we use a multi-tiered timestepping scheme, in which particles are placed onto the nearest power of two timestep based on their most recently calculated gravitational acceleration.[2]

This more efficient scheme introduces two issues, however. Firstly, momentum is not completely conserved when bodies switch timestep tiers. The error introduced becomes particularly severe for a particle on an eccentric orbit, whose perihelion and aphelion distances straddle a timestep boundary. For a large collection of particles, this problem manifests itself as the development of a V-shaped gap in the a-e plane, centered on the boundary itself. To correct this problem, we introduce a

[2] This scheme is used on almost all works using ChaNGa, and is common among large-scale simulation codes.

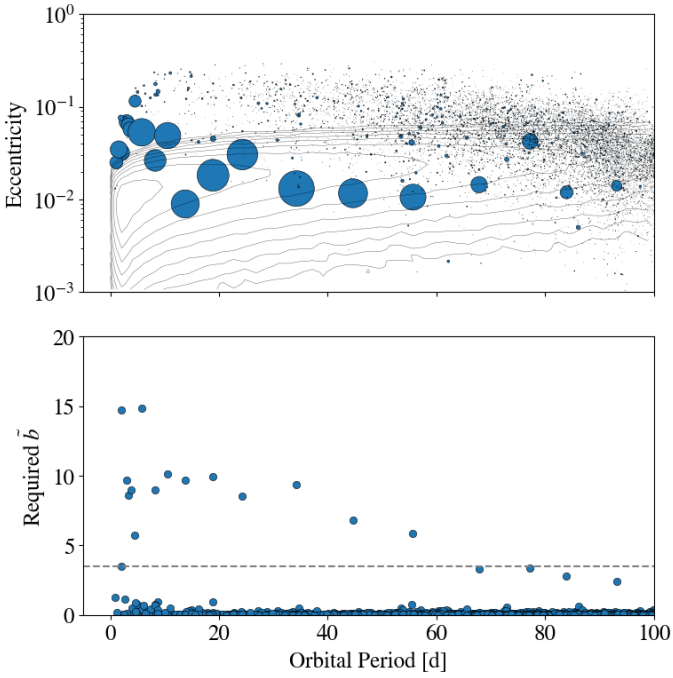

Figure 5. The final state of the fdHi simulation. In the top panel, the contours denote the initial period-eccentricity distribution of the planetesimals. Point sizes indicate the relative masses of bodies at the end of the simulation. In the bottom panel, we show the feeding zone width (see equation 11) required to produce the final masses of the bodies. The dashed line indicates the feeding zone size ($\tilde{b} = 2\sqrt{3}$) expected for bodies on circular orbits. Interior to the oligarchic growth region (around 60 d), the feeding zone sizes exceed this value.

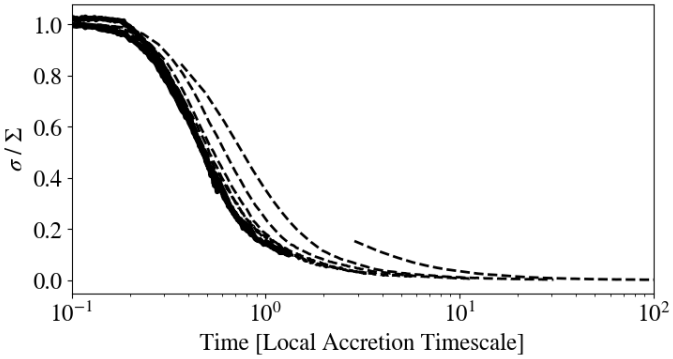

Figure 6. The time evolution of the planetesimal surface density (in units of the total solid surface density) in the fdHi simulation. Each curve represents a radial slice of the disk. The outermost region evolves the slowest, and is therefore represented by the top curve. The dashed lines indicate radial zones interior to the 60 day orbital period boundary.

Table 2. Final Properties of Full Disk Simulations

Name	M_{PP}^{a}	T_{int}^{b}	T_{int1}^{c}
fdHi	1.00	456	16,377
fdHiShallow	1.19	456	16,377
fdHiSteep	1.08	456	16,377
fdLo	1.77×10^{-3}	3,713	133,651

NOTE
[a] Maximum protoplanet mass [M_{earth}]
[b] Integration time [yr]
[c] Rescaled integration time [yr]

slightly modified timestepping criterion, which is based on the expected gravitational acceleration of the particle at pericenter. Only in the case of a close encounter with another planetesimal (in which the acceleration is no longer dominated by the star) is the timestep allowed to reduce based on the original instantaneous criterion.

A second issue is introduced when two particles on different timesteps undergo a collision. As in the previous case, momentum is not completely conserved because the most recent 'kick' steps did not happen simultaneously for these bodies. Early in the simulation, we find that this problem tends to trigger runaway growth at the timestep boundaries first. This issue carries itself forward through the embryo formation phase, and protoplanets tend to form at the boundaries. To correct this issue, we ignore collisions between bodies on different timesteps early in the simulation. We find that preventing multi-timestep collisions until after the maximum mass grows by a factor of 10 prevents any artifacts from developing at the timestep boundaries, while also minimizing the number of 'skipped' collisions.[3]

5.4. *Results*

The timescales for embryo formation depend on the chosen surface density profile, along with the local orbital timescale. Protoplanets form first at the inner edge of the disk, where the dynamical timescales are short. Growth proceeds in an inside-out fashion, with the outermost regions of the disk completing the protoplanet assembly phase last. This radial timescale dependence is not typically accounted for in planet formation simulations[4], and appears to be an important component to forming realistic solar system analogs (Clement et al. 2020). As with the narrow annulus simulations, we stop the integration once the masses of protoplanets in the

[3] In the case of fdHi, only about 20 collisions out of an eventual 900,000 are ignored.

[4] Instead, the innermost protoplanets patiently 'wait' for this phase of evolution to complete everywhere in the disk

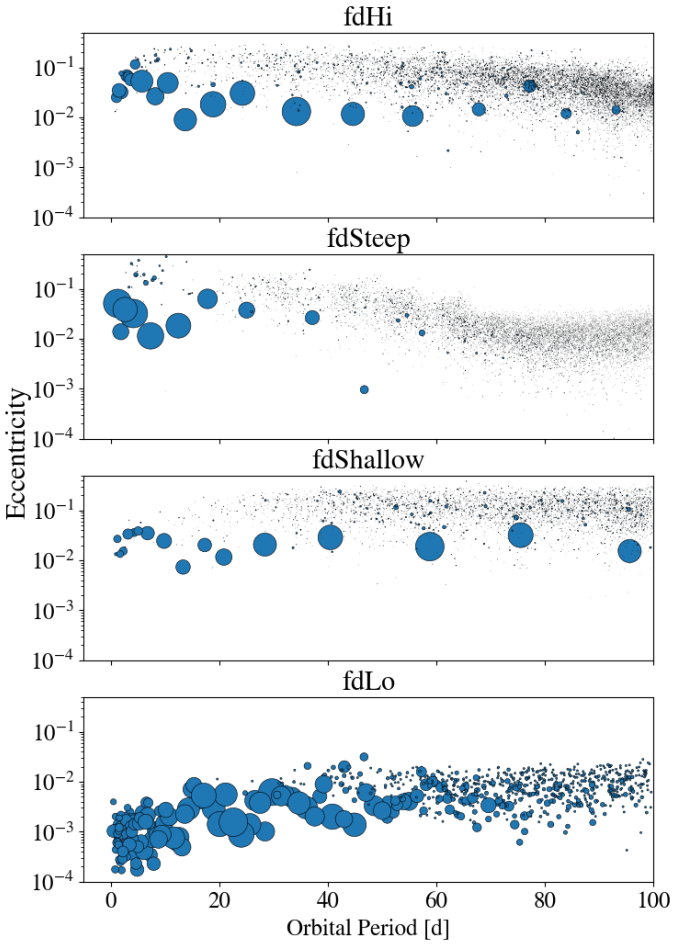

Figure 7. The final state of the full disk simulations listed in table 2. Point sizes indicate mass relative to the largest body in each simulation.

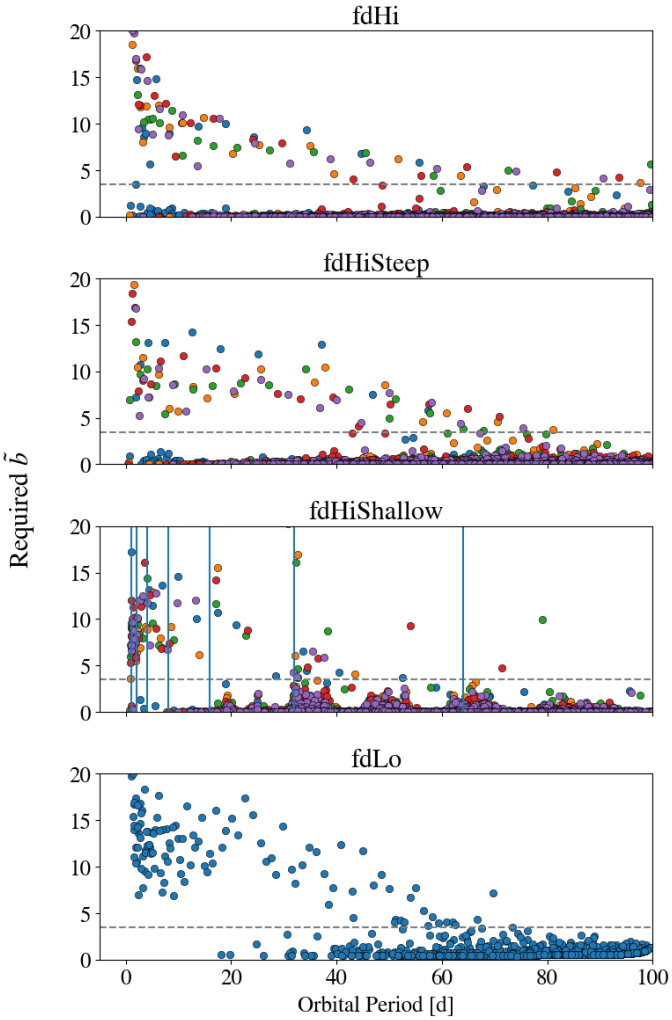

Figure 8. Feeding zone width (see equation 11) required to produce the final masses for the protoplanets from the simulations listed in table 2. The horizontal dashed line indicates $\tilde{b} = 2\sqrt{3}$. Despite the vastly different initial solid surface density profiles, the feeding zone width reaches the circular orbit value around ~ 60 days in all cases.

outermost region of the disk reach a steady value. In table 2, we summarize the outcomes of the four "full disk" cases.

We show the final state of the "fdHi" simulation in figure 5. In the top panel, the initial (contours) and final (points) state of the simulation is shown in the orbital period-eccentricity plane. The size of the points indicates the relative mass of the bodies. In the bottom panel, the final masses of the bodies (in units of feeding zone size) are shown as a function of orbital period. The feeding zone size $\tilde{b}$ is calculated according to Kokubo & Ida (2002)

$$M = \left[\frac{\left(2\pi a^2 \Sigma \tilde{b}\right)^3}{3M_*} \right]^{1/2}, \qquad (11)$$

where M is taken to be the final mass of each body. Here, we assume that each embryo has reached its isolation mass, and that differences in mass are driven by differences in the initial surface density at the embryo's current location, along with the size of its feeding zone, which is set by the dynamics relevant at that location in the disk. By plotting the derived value of $\tilde{b}$ as a function of orbital period, differences in the dynamical interactions at different locations of the disk are made more clearly visible. For two bodies on circular, non-inclined orbits, $\tilde{b} = 2\sqrt{3}$ (indicated by the horizontal dashed line) is the smallest orbital separation that produces a non-negative Jacobi energy and permits a close encounter (see Nakazawa & Ida (1988)). In typical oligarchic growth simulations (Kokubo & Ida 1998), protoplanets tend to space themselves apart by $\tilde{b} = 10$,

although it should be noted that they do not consume all of the planetesimals within this distance.

A qualitative shift in the protoplanet and planetesimal distribution is visible at $\sim$ 60 days. Interior to this location, there are very few remaining planetesimals and the embryos formed have larger feeding zones. Exterior to the boundary, the residual planetesimal population is much more visible, and protoplanets more closely follow the $\tilde{b} = 2\sqrt{3}$ line. This suggests that the transition between the low α and high α accretion modes seen in section 4 is happening near this location.

In section 4, we postulated that the increased importance of inelastic damping in the inner, non-oligarchic growth region of the disk should lower the overall eccentricity of the protoplanets there. This behavior is not immediately apparent in the top panel of figure 5. There are, however, a couple of factors in the wide disk simulations that could make this extra dynamical cooling mechanism difficult to see. Firstly, the initial eccentricity distributions of the inner and outer disk are different because of the dependence of the viscous stirring and gas drag timescales on orbital period. Additionally, the protoplanet formation timescales for the inner and outer disk are vastly different, making a comparison between these regions at the same moment in time somewhat inappropriate.

To ensure that the boundary seen near 60 days in orbital period is not simply a transient product of the inside-out growth throughout the disk, we examine the time evolution of σ/Σ, which compares the planetesimal and total solid surface density at multiple orbital periods. In figure 6, the value of σ/Σ is plotted as a function of time in 10 orbital period bins, each with a width of 10 days. Bins interior to 60 days are shown by a dashed line, while those exterior are shown as a solid line. In all radial bins, the planetesimal surface density is approaching an asymptotic value. In the inner disk, this value asymptotes to zero as the planetesimal population entirely depletes. In the outer disk, dynamical friction between the embryos and planetesimals eventually throttles subsequent accretion and leaves $\sim$ 10 percent or more of the mass surface density as planetesimals. It should be noted that in a typical oligarchic growth scenario, where protoplanets space themselves apart by 10 r_h and settle onto circular orbits (giving $\tilde{b} = 2\sqrt{3}$), roughly 30 percent of the planetesimals should remain out of reach of the protoplanets[5].

[5] A feeding zone width of $\tilde{b} = 2\sqrt{3}$ covers roughly 70 percent of the 10 r_h space between the protoplanets.

Next, we investigate how the resulting planetesimal and protoplanet distribution changes as we vary the initial solid surface density profile. The final orbital period-eccentricity state of the particles in the fdHi, fdHiSteep, fdHiShallow and fdLo simulations are shown in figure 7, with point sizes indicating the relative masses of the bodies. In all cases, the inner disk is largely depleted of planetesimals, while the outer disk contains a bimodal population of planetesimals and embryos, with a clear separation in eccentricity between the two. Despite having significantly different masses, the planetary embryos formed in all simulations have remarkably similar eccentricities. This is likely due to the fact that inelastic collisions play a more significant role where the solid surface density is highest, which offsets the fact that the initial bodies started off in a dynamically hotter state (due to the increased effectiveness of viscous stirring). The only exception to this is the fdLo simulation, where the resulting eccentricities are a couple orders of magnitude smaller. Inelastic damping likely plays an even more significant role here, due to the much larger masses of the initial planetesimals.

In figure 8, we plot the masses of the resulting protoplanets and planetesimals in all four simulations in units of $\tilde{b}$ (see equation 11). As mentioned previously, $\tilde{b} = 2\sqrt{3}$ (indicated by the horizontal dashed line) is the feeding zone width that a body on a circular orbit will have. In all four simulations, the feeding zone width exceeds the minimum value in the inner disk and approaches $2\sqrt{3}$ beyond $\sim$ 60 days. The orbital periods at which this transition occurs are quite similar between simulations, despite the vastly different solid surface density profiles used. This indicates that the boundary between accretion modes is driven entirely by the local value of α, and also supports our conclusion that planetesimal accretion is largely complete everywhere in the disk.

5.5. *Assembly History of Embryos*

Further insight regarding the difference between the short vs long period accretion modes can be gained by looking at the growth history of the planetary embryos. Because all collisions are directly resolved by the N-body code, a lineage can be traced between each planetary embryo and the initial planetesimals.

We begin by investigating the "smoothness" of the accretion events that give rise to each embryo. Drawing from a common technique used for cosmological simulations of galaxy formation, we divide growth events for a given body into "major" and "minor" mergers. Here, we define minor events as any collision involving an initial mass planetesimal, while major events consist of a

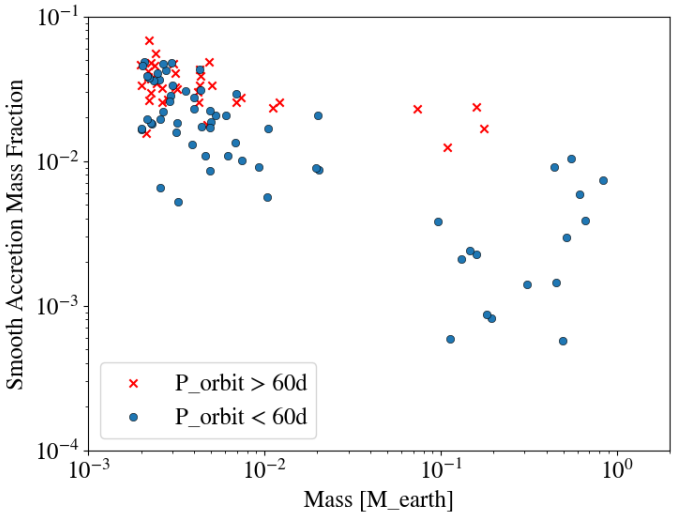

Figure 9. For the 100 most massive bodies at the end of the fdHi simulation, the fraction of their total mass attained through mergers with initial mass planetesimals (smooth accretion) as a function of total mass. Bodies that reside beyond the 60 day accretion boundary are shown with red crosses, while bodies interior to the boundary are shown with blue dots. For the short period bodies, there is a decreasing correlation between smooth accretion fraction and mass, which suggests that most growth occurs between equal mass bodies. For the bodies in the outer disk, this trend is flat, indicating that accretion of planetesimals is important during all phases of evolution.

merger between any two larger bodies. In figure 9, we choose the 100 largest bodies at the end of the fdHi simulation, retrieve all collision events involving these bodies, and plot the total mass fraction attained through minor events as a function of the final mass of the body. The bodies are then subdivided into those that end up with orbital periods greater than 60 days (red x's) and less than 60 days (blue dots). For the bodies in the outer oligarchic growth region, the trend between smooth accretion mass fraction and final mass is nearly flat. Regardless of how much an embryo has grown, mergers with initial mass planetesimals contribute on the order of a few percent to the final mass. At shorter orbital periods, however, the contribution from minor mergers can be over an order of magnitude smaller as the embryos mature.

The variation in smooth accretion fraction with mass for the short period bodies suggests that the planetesimal and embryo populations interact differently than those in the outer disk. Exterior to the 60 day accretion mode boundary, the growing embryos continue to accrete planetesimals as they near their final mass. Inside the boundary, however, later growth events tend to be dominated by embryo-embryo collisions, and the smooth accretion fraction drops as mergers with planetesimals play a less significant role. Gravitational scattering between embryos and planetesimals is a key ingredient for orbital repulsion (see Kokubo & Ida (1998)), and so a lack of gravitational scattering in the inner disk should prevent the embryos from settling onto neatly-spaced, isolated orbits. As we showed in figure 8, the embryos in the inner disk appear to reach well beyond the typical feeding zone size predicted by an oligarchic growth model. Figure 9 suggests that the extra mass here obtain comes from mergers with the other nearby embryos.

Another line of evidence pointing to a lack of gravitational scattering and orbital repulsion in the inner disk can be seen in figure 10. Here, we have chosen the 20 most massive bodies from the fdHi simulation and arranged them in order of final orbital period. On each line, the blue hash mark indicates the present orbital period of an embryo and the histogram represents the initial orbital period distribution of the planetesimals used to construct the embryo. One should note that unlike the previous figure, this plot shows where every single bit of mass (in the form of planetesimals) originated, rather than only indicating the result of direct collisions with the embryos.

Qualitatively, there are a couple of key differences between the initial planetesimal distributions in the inner (< 60 days) and outer (> 60 days) part of the disk. The planetesimal distributions for the outer disk are much more smooth and unimodal, while many of the distributions near the inner disk rather disjoint. As discussed when examining figure 9, growth events for the inner embryos tend to be sudden and stochastic, often involving mergers with other embryos. When an embryo-embryo collision happens, one would expect a second peak to appear in the accretion distribution as the merger tree suddenly obtains a whole other subtree from the embryo that it absorbed. In the outer disk, however, the increased importance of embryo-planetesimal mergers means that growth should be smooth, steady and local.

In figure 10, evidence of orbital repulsion can be seen for the outermost embryos. Beyond 60 days, the final positions of the embryos tend to be offset from the peaks of the accretion distributions. This suggests that gravitational scattering events between embryos occurred later on, after accretion had mostly completed. Although many of the inner embryos also end up shifted away from the peak of their accretion distribution, their present position is usually associated with another secondary peak. This suggests that most of the close encounters between embryos here resulted in a merger event, rather than a scatter.

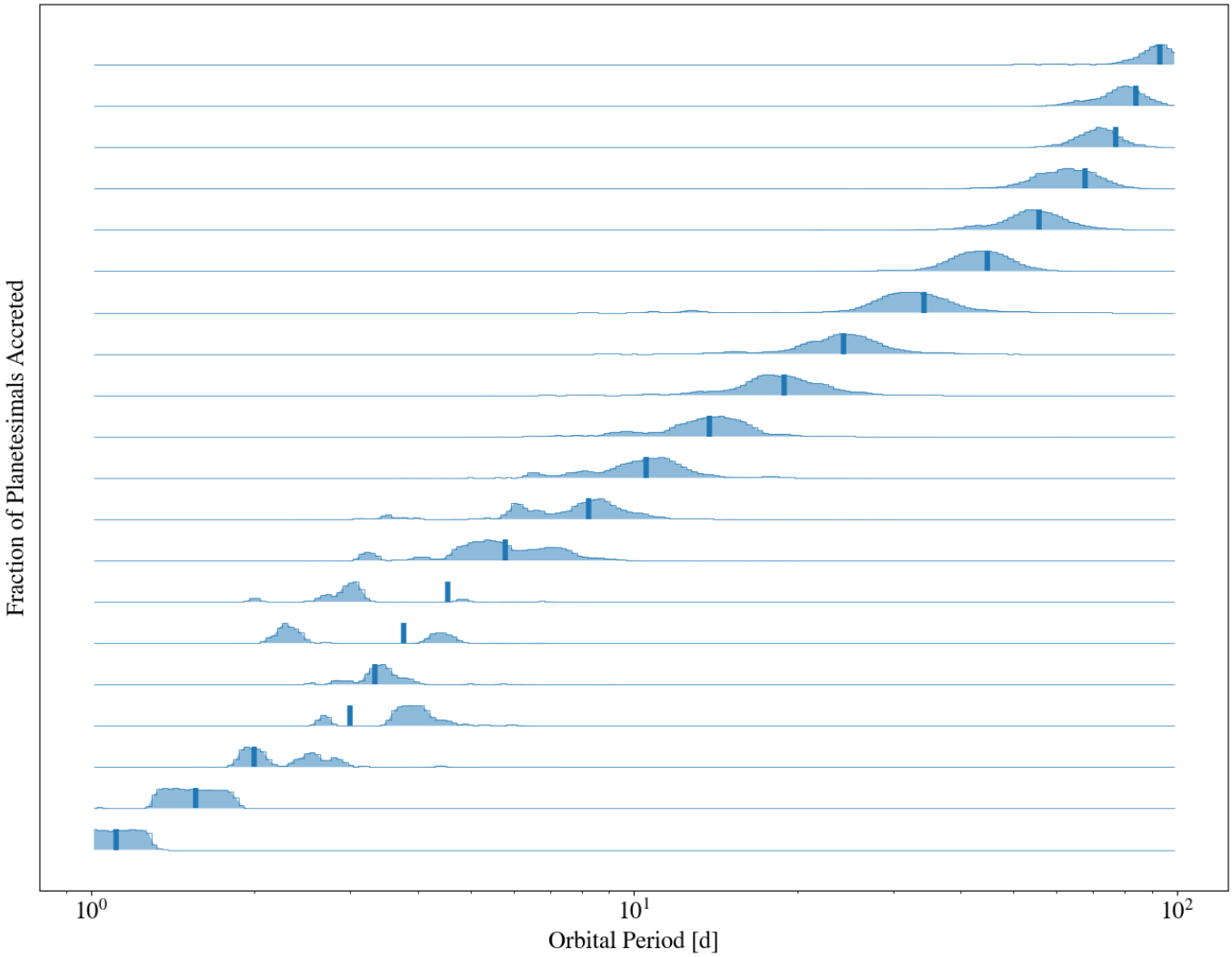

Figure 10. For the 20 most massive bodies at the end of the fdHi simulation, the relative shape of the accretion zones for each body are shown. The hash marks indicate the present position of the body. The histograms indicate the initial locations of the planetesimals that were used to assemble a body.

6. SIMPLIFYING ASSUMPTIONS

6.1. *Collision Cross Section*

In all cases shown so far, the boundary between the oligarchic growth and the highly-efficient short period accretion region lies around 60 days in orbital period. As discussed in section 2.2, the mode of accretion is set entirely by the local value of α, which scales with both distance from the star and the bulk density of the planetesimals (see equation 4). Because we chose to artificially inflate the collision cross section of the particles in our simulations, the bulk densities of the particles are reduced, and the accretion boundary is shifted outward. However, the scaling relation between α and ρ ($\alpha \sim \rho_{\rm pl}^{-1/3}$) can be used to predict where this accretion boundary should lie in a disk with realistic-sized planetesimals. The simulations presented in this paper use a collision cross section enhancement factor of 6, which moves the boundary outward in orbital period by a factor of approximately 15. One would therefore expect the accretion boundary to lie near 5 days in orbital period for 3 g cm^{-3} bodies.

Although a simulation with f = 1 is not computationally tractable, we can test whether the accretion boundary moves in the way we expect by modestly changing the value of f. In figure 11, we compare the fdHi simulation to a nearly identical run using f = 4. In the top panel, we show the feeding zone width required for each particle to attain its present mass. As in figure 8, we indicate the feeding zone size expected for oligarchic growth with a horizontal dashed line. In the bottom panel, the value of α as a function of orbital period is

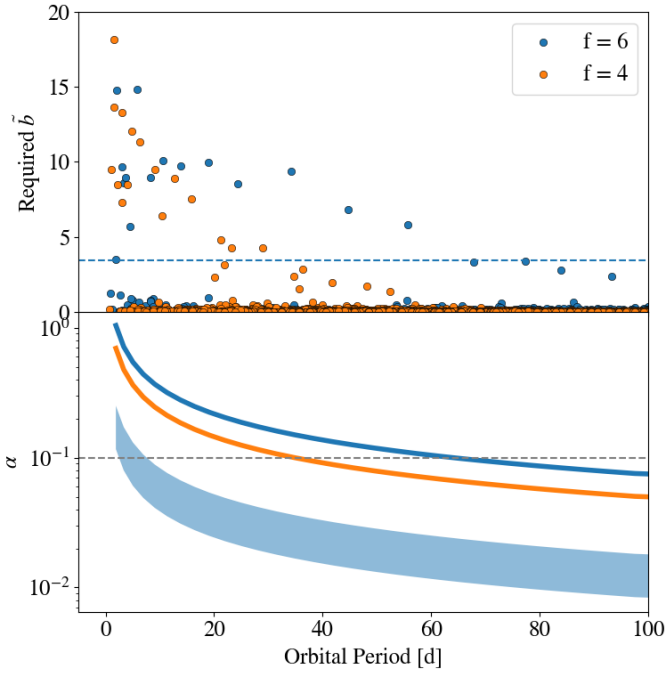

Figure 11. In the top panel, we show the required feeding zone sizes to produce the masses of the bodies seen at the end of the fdHi and fdHif4 simulations. The bottom panel shows the variation of α with orbital period for the bodies used in each case (solid curves). The orbital period at which $\alpha \simeq 0.1$ matches well with the location at which $\tilde{b}$ exceeds $2\sqrt{3}$. The shaded region in the bottom panel show the values of alpha for realistic-sized (f = 1) planetesimals with bulk densities between 10 and 1 g cm^{-3}.

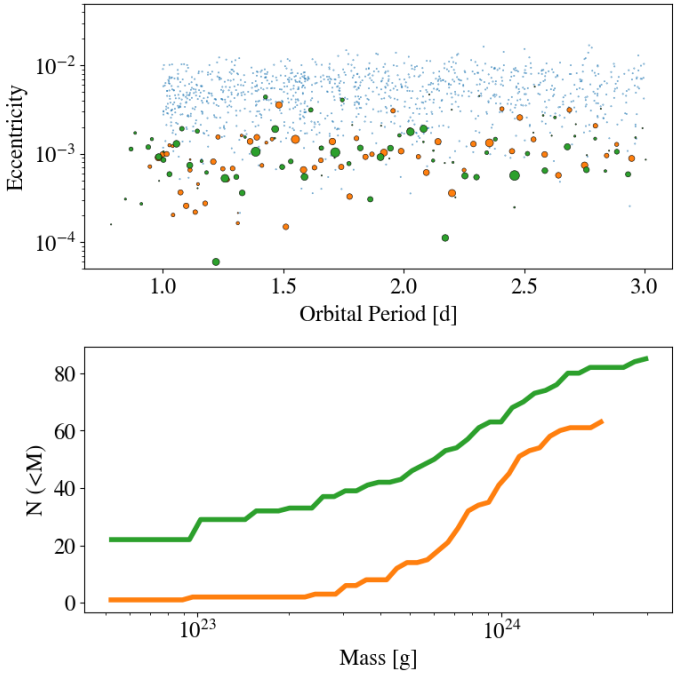

Figure 12. A comparison between the innermost region of the fdLo (orange) simulation, and a second version using a bounce- merge collision model (green). In the top panel, the period-eccentricity state of the particles is shown, with marker sizes indicating relative mass. The blue points represent the initial state of the simulations. The bottom panel compares the final cumulative mass distributions of the bodies.

shown for 3 g cm^{-3} bodies with an artificial radius enhancement of f = 1, 4 and 6. The horizontal dashed line indicates the empirical value of alpha below which the accretion mode switches to oligarchic. Comparing the top and bottom panels, the intersection of the feeding zone width seen in our simulations and the feeding zone width predicted by oligarchic growth matches well with the orbital period at which $\alpha \sim 0.1$ for both values of f. Also shown by the shaded region are the expected α values for realistic-sized bodies with ρ_{pl} between 1 and 10 g cm^{-3}. Although the removal of the cross section enhancement greatly reduces the size of the non-oligarchic region, it still should be expected to cover a portion of the disk where planetesimals might be expected to form for a wide range of ρ_{pl}.

6.2. *Collision Model*

For the simulations presented in this work, every collision results in a perfect merger between pairs of bodies, with no loss of mass or energy. Although simpler and less computationally expensive to model, allowing every collision to produce a perfect merger might result

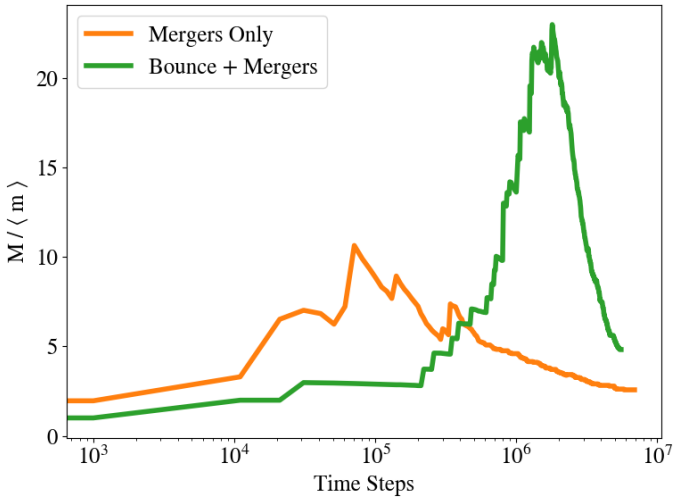

Figure 13. The evolution of the ratio between the maximum and mean mass of the simulations shown in figure 12. In both cases, the system first evolves through a phase of runaway growth, before the massive bodies consume the smaller bodies, driving down the mean mass. With the bounce-merge model, the mass ratio takes much longer to begin decreasing.

in overly efficient growth, particularly in the innermost region of the disk where the encounter velocities are largest. A proper way to handle this would be to allow for a range of collision outcomes, based on a semianalytic model (see Leinhardt & Stewart (2012)). However, resolving collisional debris, or even prolonging growth by forcing high-velocity pairs of bodies to bounce is too expensive to model, even with ChaNGa.

To test whether a more restrictive collision model should alter the growth mode of the inner disk, we ran a smaller scale test using a more restrictive collision model. In this case, a collision can result in one of two outcomes: if the impact velocity is smaller than the mutual escape velocity of the colliding particles, defined as

$$v_{mut,esc} = \sqrt{\frac{2G(m_1 + m_2)}{r_1 + r_2}}, \tag{12}$$

where m_1, m_2 and r_1, r_2 are the masses and radii of colliding particles 1 and 2, then the bodies merge. For impact velocities larger than $v_{mut,esc}$, no mass is transferred, and the bodies undergo a completely elastic bounce. Because the accretion outcome is all or nothing, this model should restrict growth more than a partial accretion model (Leinhardt & Stewart 2012). Below, we will show that the bounce-merge model does not meaningfully affect the outcome of the inner disk's planetesimal accretion phase, and so a more realistic partial accretion model should do the same.

To compare the outcome of the two collision models, we have chosen to use the initial conditions from the fdLo simulation, but have truncated the disk beyond 3 days in orbital period. This offsets the increased computational cost of the more restrictive collision model, while still allowing the disk to evolve in the region where mergers would be most difficult to achieve. For the initial conditions we have chosen, the typical encounter velocity (defined by $v_{enc} = \langle e^2 \rangle^{1/2} v_k$, where v_k is the local Keplerian velocity) is about 25 percent larger than $v_{mut,esc}$. Because the encounter velocities follow a Gaussian distribution, there should still be a small subset of collisions that still meet the merger criteria to occur early on. In addition, $v_{mut,esc}$ becomes larger as the bodies grow and the merger criteria should become easier to meet as the system evolves. For these reasons, one would expect the inhibition of growth due to the more restrictive collision model to be temporary.

In figure 12, we compare the outcomes of the simulations, one with mergers only (shown in orange) and one with the bounce-merge model (shown in green). The blue points in the top panel show the initial conditions used for both cases. Although the bounce-merge simulation takes much longer to reach the same phase of evolution, the resulting orbital properties and mass distribution (with the exception of some extra residual planetesimals) are indistinguishable from the merger-only case.

To investigate the differences in growth between the two collision models early on, we show the time evolution of the ratio between the maximum and mean mass in figure 13. In both cases, this ratio first increases, which indicates that runaway growth still operates, regardless of the collision model used. In the bounce-merge case, the mass ratio peaks at a higher value, while also undergoing a longer runaway growth phase. This suggests that the mass distribution becomes much less unimodal during this growth process, but as figure 12 shows, this does not affect the resulting embryos or allow for a residual planetesimal population.

As a final note, Childs & Steffen (2022) found that a more realistic collision model also enhanced radial mixing in their simulations. Upon calculating the planetesimal accretion zones using the same method as was done to produce figure 10, we find that the embryos in the bounce-merge simulation annulus do have modestly wider accretion zones than those produced in the merger-only simulation.

7. SUMMARY AND DISCUSSION

In this work, we have demonstrated that planetary embryo growth can simultaneously operate in two distinct modes in a planet-forming disk. In the first mode, gravitational feedback from the growing embryos heats the remaining planetesimals and results in a dynamically cold population of embryos with a modest amount of residual planetesimals. This corresponds to the "oligarchic growth" case revealed by (Kokubo & Ida 1998), which is often used as a starting point for late-stage accretion models (e.g. Kokubo & Ida (2002); Raymond et al. (2005, 2006)). In the second mode, the gravitational feedback does not operate, embryos quickly sweep up all planetesimals, and grow larger and less uniformly spaced than those produced by oligarchic growth. The distinction between these modes is determined by the ratio between the physical size of the bodies and their Hill radius, which sets the relative contribution of close gravitational encounters and collisions to the dynamical evolution of the disk.

We have demonstrated the outcome of both accretion modes through a simple parameter study using a narrow annulus of planetesimals. The initial planetesimal distribution can be described in terms of two dimensionless constants, α and β, which describe the ratio between the physical radius of the planetesimals and the Hill (r_h) and gravitational (r_g) radius, respectively. For a fixed planetesimal composition, α scales with the orbital period

and β scales with the level of dynamical excitation of the disk. We showed that $\alpha \ll 1$ leads to oligarchic growth, while a non-negligible α produces this newly revealed non-oligarchic growth mode. Within this non-oligarchic mode, we find that the resulting masses and eccentricities of the embryos come out the same, regardless of the initial value of β.

So long as the density of the bodies do not significantly change as their mass distribution evolves, this ratio, and therefore the location of the boundary between these accretion modes is set entirely by the distance from the star. Because both the physical and Hill radii of the bodies grows as $M^{1/3}$, the growth mode boundary remains stationary in the disk during the planetesimal accretion process.

We have verified that the growth boundary location is independent of the solid surface density distribution by testing the outcome of the planetesimal accretion process for a variety of solid profiles. Although altering the surface density does affect the resulting masses of the embryos, the location of the boundary separating the growth modes is remarkably similar among all of our simulations. In addition, the sizes of the feeding zones, along with qualitative differences in the accretion history of embryos on both sides of the boundary provide further evidence to suggest that oligarchic growth is not operating in the inner disk.

Finally, we examined the way in which our simplifying assumption of perfect accretion, along with the enhancement of the collision cross sections to speed up the simulations might alter the emergence and location of the non-oligarchic growth region. We showed that a much more restrictive collision model, in which only low-velocity collisions produce a merger, still allows for this growth mode to occur at the innermost part of the disk, where encounter speeds are most vigorous. In a real planet-forming disk, partial accretion events should allow growth to happen more quickly than what was seen in this test case, so this growth mode should certainly still occur. We also showed that the collision cross section enhancement moves the accretion boundary outward. We verified this by deriving a scaling relation between the boundary location and the bulk density of the planetesimals, and showing that the boundary moves to the predicted location when running a simulation with a slightly smaller inflation factor. For rocky planetesimals with a realistic bulk density, this boundary should lie around 5 days in orbital period.

To date, there have been no other studies of planetesimal accretion with such a large value of α. However, a value of $\alpha = 1$ corresponds to the Roche limit of a three-body system, and so one might wonder this high-α accretion mode might be relevant for a circumplanetary accretion. There is a small collection of previous works which use N-body methods to examine in-situ satellitesimal accretion (Ida et al. 1997; Richardson et al. 2000; Kokubo et al. 2000; Ida et al. 2020), although some of these simulations involve a complex interaction between spiral density waves formed inside of the Roche limit and the material exterior to it. Ida et al. (1997) was able to form 1-2 large moons just exterior to the Roche limit, depending on the extent of the disk with very little satellitesimal material left over. The widest disk they modeled extended out to $\alpha = 0.5$. Qualitatively, this result is very similar to the short period planetesimal accretion mode observed in our simulations. Ida et al. (2020) modeled a much wider satellitesimal disk, which extends out to about $\alpha \approx 0.05$. Inside to the $\alpha = 0.1$ accretion boundary (which lies near $15R_U$ in figure 1 of Ida et al. (2020)), bodies grow beyond the isolation mass, while the opposite is true on the other side of the boundary. In addition, a residual population of satellitesimals is still present beyond the boundary, which suggests that oligarchic growth is indeed operating only on the far side.

Presently, the implications that this non-oligarchic accretion mode has for the formation of short-period terrestrial planets, and whether the accretion boundary would leave any lasting imprint on the final orbital architecture, is unclear. The extreme efficiency of planetesimal accretion at the inner edge of the disk suggests that no residual populations of small bodies should be expected to exist here. A crucial point that our results do highlight is that the initial conditions used for most late-stage planet formation simulations are overly simplistic. Clement et al. (2020) recently simulated planetesimal accretion in a disk extending from the orbit of Mercury to the asteroid belt and found that the disk never reaches a state in which equally-spaced, isolation mass embryos are present everywhere simultaneously. Instead, different annuli reach a 'giant impact' phase at different times, preventing the onset of a global instability throughout the entire disk, as is common in classic terrestrial planet formation models (Chambers & Wetherill 2001; Raymond et al. 2009).

To connect these accretion modes to the final orbital architecture, and to ultimately determine what implications an in-situ formation model has for the growth of STIPs, we will evolve the final simulation snapshots presented here with a hybrid-symplectic integrator for Myr timescales. The final distribution of planets formed, along with composition predictions generated by applying cosmochemical models to our initial planetesimal

distributions and propagating compositions through the collision trees, will be examined in a follow-up paper.

ACKNOWLEDGEMENTS

This work used the Extreme Science and Engineering Discovery Environment (XSEDE), which is supported by National Science Foundation grant number ACI-1548562. SCW and TRQ were were supported by National Science Foundation grant number AST-2006752. We acknowledge the people of the Dkhw'Duw'Absh, the Duwamish Tribe, the Muckleshoot Tribe, and other tribes on whose traditional lands we have performed this work.

Software: Astropy (Astropy Collaboration et al. 2013), ChaNGa (Jetley et al. 2008; Menon et al. 2015), Matplotlib (Hunter 2007), NumPy (van der Walt et al. 2011), Pandas (Wes McKinney 2010), PYNBODY (Pontzen et al. 2013)

DATA AVAILABILITY

The data presented in this article are available on our GitHub repository, at https://github.com/spencerw/stip_planetesimal_paper.

APPENDIX

A. ROBUSTNESS OF TIMESTEPPING SCHEME

As described in section 3, ChaNGa evolves the motions of the particles in the planetesimal disk using a multi-tiered timestepping scheme. Due to the extremely short dynamical timescale at the inner edge of the disk, the outer disk would require a prohibitive number of timesteps to reach the protoplanet phase using a fixed timestep scheme.To circumvent this, particles are evolved in discrete power-of-two timestep groups. In the event that a collision occurs between two particles on different timesteps, a slight error is introduced to the energy and angular momentum of the merged particle. Due to the nonlinear nature of the runaway growth phase, this slight error tends to trigger more subsequent collisions at the timestep boundary in the disk, and causes protoplanets to preferentially form at the boundaries.

To circumvent this issue, we prohibit particles on different timesteps from merging until the runaway growth phase is well underway. For the fdHi simulation, multi-tiered mergers are not allowed during the first thousand steps. To verify that this technique does not alter the resulting protoplanet distribution in any meaningful way, we ran two test simulations of the inner part (1 to 4 days in orbital period) of the disk from the fdHi simulation. In the first case, the aforementioned timestepping scheme is used. In the second case, all particles are evolved on the timestep appropriate for the inner edge of the disk.

In figure 14, we compare the final period-eccentricity state and final mass distributions to each other. There do not appear to be any differences between the two protoplanet distributions, particularly near the timestep boundary at 2 days. In addition, the masses of both the protoplanets and the remaining growing planetesimals are indistinguishable. We therefore safely conclude that the timestepping scheme used in this work does not alter the growth of the protoplanets in any meaningful way.

REFERENCES

Adachi, I., Hayashi, C., & Nakazawa, K. 1976, Progress of Theoretical Physics, 56, 1756, doi: 10.1143/PTP.56.1756

Agol, E., Dorn, C., Grimm, S. L., et al. 2021, PSJ, 2, 1, doi: 10.3847/PSJ/abd022

Andrews, S. M., & Williams, J. P. 2005, ApJ, 631, 1134, doi: 10.1086/432712

Astropy Collaboration, Robitaille, T. P., Tollerud, E. J., et al. 2013, A&A, 558, A33, doi: 10.1051/0004-6361/201322068

Bai, X.-N., & Stone, J. M. 2010, ApJ, 722, 1437, doi: 10.1088/0004-637X/722/2/1437

Barnes, R., Quinn, T. R., Lissauer, J. J., & Richardson, D. C. 2009, Icarus, 203, 626, doi: 10.1016/j.icarus.2009.03.042

Beitz, E., Güttler, C., Blum, J., et al. 2011, ApJ, 736, 34, doi: 10.1088/0004-637X/736/1/34

Birnstiel, T., Fang, M., & Johansen, A. 2016, SSRv, 205, 41, doi: 10.1007/s11214-016-0256-1

Bitsch, B., Lambrechts, M., & Johansen, A. 2015, A&A, 582, A112, doi: 10.1051/0004-6361/201526463

Blum, J., & Münch, M. 1993, Icarus, 106, 151, doi: 10.1006/icar.1993.1163

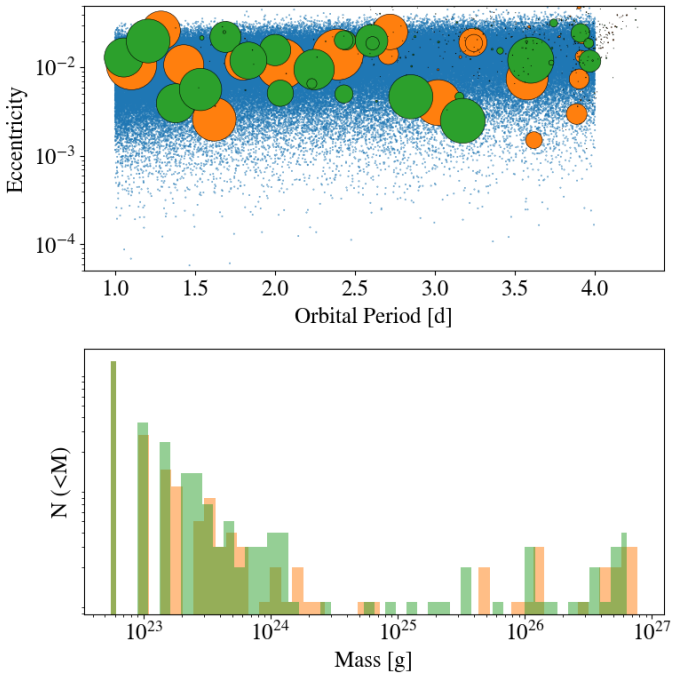

Figure 14. A comparison between the innermost region of the fdHi (orange) simulation, and a second version using a fixed timestep appropriate for the inner edge of the disk (green). In the top panel, the period-eccentricity state of the particles is shown, with marker sizes indicating relative mass. The blue points represent the initial state of the simulations. The bottom panel compares the final mass distributions of the bodies (diff or cumulative?).

Bottke, W. F., Durda, D. D., Nesvorný, D., et al. 2005, Icarus, 179, 63, doi: 10.1016/j.icarus.2005.05.017

Chambers, J. E., & Wetherill, G. W. 1998, Icarus, 136, 304, doi: 10.1006/icar.1998.6007

—. 2001, M&PS, 36, 381, doi: 10.1111/j.1945-5100.2001.tb01881.x

Childs, A. C., & Steffen, J. H. 2022, MNRAS, 511, 1848, doi: 10.1093/mnras/stac158

Clement, M. S., Kaib, N. A., & Chambers, J. E. 2020, PSJ, 1, 18, doi: 10.3847/PSJ/ab91aa

Colwell, J. E. 2003, Icarus, 164, 188, doi: 10.1016/S0019-1035(03)00083-6

Fabrycky, D. C., Lissauer, J. J., Ragozzine, D., et al. 2014, ApJ, 790, 146, doi: 10.1088/0004-637X/790/2/146

Gillon, M., Jehin, E., Lederer, S. M., et al. 2016, Nature, 533, 221, doi: 10.1038/nature17448

Gillon, M., Triaud, A. H. M. J., Demory, B.-O., et al. 2017, Nature, 542, 456, doi: 10.1038/nature21360

Hansen, B. M. S., & Murray, N. 2012, ApJ, 751, 158, doi: 10.1088/0004-637X/751/2/158

Hayashi, C. 1981, Progress of Theoretical Physics Supplement, 70, 35, doi: 10.1143/PTPS.70.35

Hunter, J. D. 2007, Computing in Science and Engineering, 9, 90, doi: 10.1109/MCSE.2007.55

Ida, S. 1990, Icarus, 88, 129, doi: 10.1016/0019-1035(90)90182-9

Ida, S., Canup, R. M., & Stewart, G. R. 1997, Nature, 389, 353, doi: 10.1038/38669

Ida, S., Kokubo, E., & Makino, J. 1993, MNRAS, 263, 875, doi: 10.1093/mnras/263.4.875

Ida, S., & Makino, J. 1993, Icarus, 106, 210, doi: 10.1006/icar.1993.1167

Ida, S., Ueta, S., Sasaki, T., & Ishizawa, Y. 2020, Nature Astronomy, 4, 880, doi: 10.1038/s41550-020-1049-8

Izidoro, A., Bitsch, B., Raymond, S. N., et al. 2021, A&A, 650, A152, doi: 10.1051/0004-6361/201935336

Izidoro, A., Ogihara, M., Raymond, S. N., et al. 2017, MNRAS, 470, 1750, doi: 10.1093/mnras/stx1232

Jetley, P., Gioachin, F., Mendes, C. Kale, L., & Quinn, T. 2008, Proceedings of IEEE International Parallel and Distributed Processing Symposium

Johansen, A., Blum, J., Tanaka, H., et al. 2014, in Protostars and Planets VI, ed. H. Beuther, R. S. Klessen, C. P. Dullemond, & T. Henning, 547

Johansen, A., Oishi, J. S., Mac Low, M.-M., et al. 2007, Nature, 448, 1022, doi: 10.1038/nature06086

Kokubo, E., & Ida, S. 1995, Icarus, 114, 247, doi: 10.1006/icar.1995.1059

—. 1996, Icarus, 123, 180, doi: 10.1006/icar.1996.0148

—. 1998, Icarus, 131, 171, doi: 10.1006/icar.1997.5840
—. 2000, Icarus, 143, 15, doi: 10.1006/icar.1999.6237
—. 2002, ApJ, 581, 666, doi: 10.1086/344105
Kokubo, E., Ida, S., & Makino, J. 2000, Icarus, 148, 419, doi: 10.1006/icar.2000.6496
Lambrechts, M., & Johansen, A. 2012, A&A, 544, A32, doi: 10.1051/0004-6361/201219127
—. 2014, A&A, 572, A107, doi: 10.1051/0004-6361/201424343
Latham, D. W., Rowe, J. F., Quinn, S. N., et al. 2011, ApJL, 732, L24, doi: 10.1088/2041-8205/732/2/L24
Leinhardt, Z. M., & Stewart, S. T. 2012, ApJ, 745, 79, doi: 10.1088/0004-637X/745/1/79
Levison, H. F., Morbidelli, A., Tsiganis, K., Nesvorný, D., & Gomes, R. 2011, AJ, 142, 152, doi: 10.1088/0004-6256/142/5/152
Levison, H. F., Morbidelli, A., Van Laerhoven, C., Gomes, R., & Tsiganis, K. 2008, Icarus, 196, 258, doi: 10.1016/j.icarus.2007.11.035
Lissauer, J. J. 1987, Icarus, 69, 249, doi: 10.1016/0019-1035(87)90104-7
Lissauer, J. J., & Stewart, G. R. 1993, in Protostars and Planets III, ed. E. H. Levy & J. I. Lunine, 1061
Lissauer, J. J., Ragozzine, D., Fabrycky, D. C., et al. 2011, ApJS, 197, 8, doi: 10.1088/0067-0049/197/1/8
Lyra, W., Johansen, A., Klahr, H., & Piskunov, N. 2008, A&A, 491, L41, doi: 10.1051/0004-6361:200810626
Menon, H., Wesolowski, L., & Zheng, G. e. a. 2015, Computational Astrophysics and Cosmology, 2, 1
Morbidelli, A., Bottke, W. F., Nesvorný, D., & Levison, H. F. 2009, Icarus, 204, 558, doi: 10.1016/j.icarus.2009.07.011
Morishima, R., Stadel, J., & Moore, B. 2010, Icarus, 207, 517, doi: 10.1016/j.icarus.2009.11.038
Nakagawa, Y., Sekiya, M., & Hayashi, C. 1986, Icarus, 67, 375, doi: 10.1016/0019-1035(86)90121-1
Nakazawa, K., & Ida, S. 1988, Progress of Theoretical Physics Supplement, 96, 167, doi: 10.1143/PTPS.96.167
Pontzen, A., Roškar, R., Stinson, G., & Woods, R. 2013, pynbody: N-Body/SPH analysis for python. http://ascl.net/1305.002
Raymond, S. N., O'Brien, D. P., Morbidelli, A., & Kaib, N. A. 2009, Icarus, 203, 644, doi: 10.1016/j.icarus.2009.05.016
Raymond, S. N., Quinn, T., & Lunine, J. I. 2005, ApJ, 632, 670, doi: 10.1086/433179
—. 2006, Icarus, 183, 265, doi: 10.1016/j.icarus.2006.03.011
Raymond, S. N., Scalo, J., & Meadows, V. S. 2007, ApJ, 669, 606, doi: 10.1086/521587
Richardson, D. C. 1994, MNRAS, 269, 493, doi: 10.1093/mnras/269.2.493
Richardson, D. C., Quinn, T., Stadel, J., & Lake, G. 2000, Icarus, 143, 45, doi: 10.1006/icar.1999.6243
Rowe, J. F., Bryson, S. T., Marcy, G. W., et al. 2014, ApJ, 784, 45, doi: 10.1088/0004-637X/784/1/45
Safronov, V. S. 1969, Evoliutsiia doplanetnogo oblaka.
Sheppard, S. S., & Trujillo, C. A. 2010, ApJL, 723, L233, doi: 10.1088/2041-8205/723/2/L233
Stewart, G. R., & Ida, S. 2000, Icarus, 143, 28, doi: 10.1006/icar.1999.6242
van der Walt, S., Colbert, S. C., & Varoquaux, G. 2011, Computing in Science and Engineering, 13, 22, doi: 10.1109/MCSE.2011.37
Wallace, S. C., & Quinn, T. R. 2019, MNRAS, 489, 2159, doi: 10.1093/mnras/stz2284
Weidenschilling, S. J. 1977, MNRAS, 180, 57, doi: 10.1093/mnras/180.2.57
—. 1989, Icarus, 80, 179, doi: 10.1016/0019-1035(89)90166-8
Wes McKinney. 2010, in Proceedings of the 9th Python in Science Conference, ed. Stéfan van der Walt & Jarrod Millman, 56 – 61
Wetherill, G. W., & Stewart, G. R. 1989, Icarus, 77, 330, doi: 10.1016/0019-1035(89)90093-6